Wall-stress modeling for laminar boundary layers in coarse grids

By C. A. Gonzalez, M. Karp† AND P. Moin

1. Motivation and objectives

As described in NASA's CFD Vision 2030 Study (Slotnick *et al.* 2014), for external aerodynamic applications such as flow over an airfoil, the number of computational volumes in the laminar and transitional regions can exceed that of the turbulent region by up to two orders of magnitude in a wall-modeled large-eddy simulation (WMLES). The associated high computational cost is a key bottleneck in the application of such reduced-order models. The flow in the vicinity of a wing's leading edge is commonly characterized by an extremely thin boundary layer, on the order of 1 mm at $Re_c = 10^8$, subject to a favorable pressure gradient. This laminar boundary layer is under-resolved for the grid resolutions typically used for WMLES calculations. Though the extent of the laminar region is small, usually only a few percent of the chord, the associated problems with under-resolving this region of the flow can be nonnegligible. Investigations on a NACA0012 airfoil have shown that the flow prediction along the chord of the airfoil can be dramatically affected by the grid resolution at the leading edge, as shown in Figure 1. When the leading-edge flow is under-resolved, the downstream propagation of the incurred errors in the flow leads to spurious leading-edge separation, as well as affecting lift, drag, and surface pressure along the full airfoil. The goal of this investigation is to develop a wall model capable of treating the laminar region of the flow without the need to fully resolve it. This will allow the use of relatively coarse grids, such as the ones commonly utilized in WMLES calculations, in the laminar region without compromising the accuracy of the solution. Other formulations of this problem have focused on using data-driven models (Marques & Wang 2017) and integral methods (Drela & Giles 1987). Here, we derive an expression for the wall shear stress from the Falkner-Skan similarity solutions for wedge flows and demonstrate that it can be successfully used as a wall-stress model for coarse laminar simulations. It is applied to two preliminary cases: 1) stagnation flow and 2) boundary layer flow with an injection boundary condition used to generate a favorable streamwise-varying pressure gradient.

2. Methodology

2.1. *Model formulation*

The flow over the top of a wedge can be modeled as an external flow $U_e(x)$ with a pressure gradient given by the inviscid flow solution, under the assumption $Re \gg 1$. The angle of the wedge is given as $\beta\pi$. The external flow velocity, U_e, is given by

$$U_e(x) = kx^m, \tag{2.1}$$

† Presently at Technion, Israel.

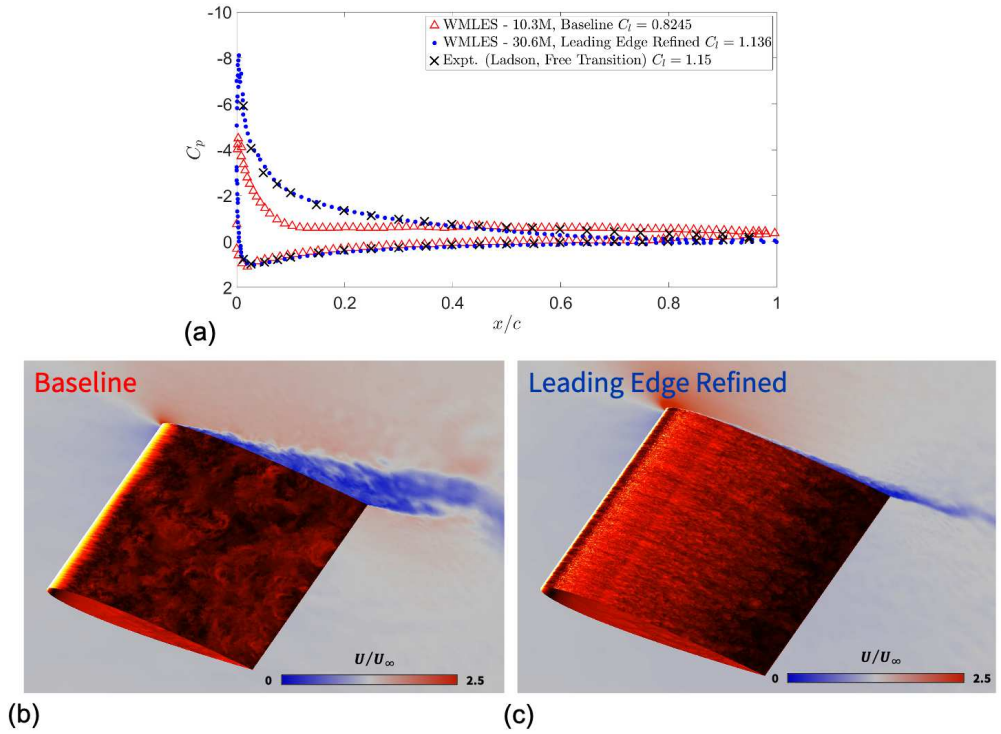

FIGURE 1. Effect of leading-edge resolution on WMLES of the NACA0012 at $AoA = 15$ degrees, $Re_c = 3M$, and $Ma_\infty = 0.3$, adapted from Goc *et al.* (2020). (a) Sectional surface pressure coefficient for the two grids compared with experimental data from Ladson *et al.* (1987). (b) WMLES baseline grid resolution (10M control volumes). (c) WMLES with $\times 4$ leading-edge grid resolution refinement (30.6M).

where x is the streamwise surface coordinate along the wedge. The coefficient k is proportional to the strain rate and is therefore a function of the flow geometry. The exponent m is a function of β and is given by

$$m = \frac{\beta}{2 - \beta}. \tag{2.2}$$

The flow near the wedge is governed by the boundary layer equations. The equation for continuity is

$$\frac{\partial u}{\partial x} + \frac{\partial v}{\partial y} = 0, \tag{2.3}$$

where y is the wall-normal coordinate, and (u, v) are the velocities along (x, y), respectively. For steady flow in a boundary layer, the x-momentum equation is given by

$$u\frac{\partial u}{\partial x} + v\frac{\partial u}{\partial y} = -\frac{1}{\rho}\frac{\mathrm{d}P(x)}{\mathrm{d}x} + \nu\frac{\partial^2 u}{\partial y^2}, \tag{2.4}$$

where ρ is the fluid density and ν is the kinematic viscosity. The streamwise momentum equation in the outer inviscid region relates the pressure gradient to the external velocity

$$U_e \frac{\mathrm{d}U_e}{\mathrm{d}x} = -\frac{1}{\rho}\frac{\mathrm{d}P(x)}{\mathrm{d}x}. \tag{2.5}$$

The boundary layer equations can then be reduced to an ordinary differential equation using the similarity solution developed by Falkner and Skan (White & Corfield 2006). The similarity coordinate η is formed as

$$\eta = y\sqrt{\frac{m+1}{2}\frac{U_e(x)}{\nu x}}. \tag{2.6}$$

The nondimensional velocities are given as

$$u^* = \frac{u}{U_e(x)} = f'(\eta) \tag{2.7}$$

and

$$v^* = \frac{v}{U_e(x)} = f(\eta) - \frac{m-1}{m+1}\eta f'(\eta). \tag{2.8}$$

The governing equation for f can be found by substituting these nondimensional terms into the x-momentum equation

$$f''' + ff'' + \beta\left[1 - (f')^2\right] = 0, \tag{2.9}$$

subject to the following boundary conditions

$$f(0) = f'(0) = 0, \quad f'(\infty) = 1. \tag{2.10}$$

Lastly, it is useful to write an expression for the wall shear stress,

$$\tau_w = \mu\sqrt{\frac{m+1}{2}\frac{U_e(x)^3}{\nu x}}f''(0). \tag{2.11}$$

We propose to model the subgrid laminar boundary layer at each streamwise location along the surface of the wall as a local Falkner-Skan boundary layer. As such, we need to extract the coefficients characterizing this boundary layer at each streamwise location. Therefore, the flow solver needs to calculate $U_e(x)$, $m(x)$, and $f''(0)(x)$ at all streamwise locations. One can formulate a linear system to solve for $m(x_i)$ and $k(x_i)$, where i is the wall-tangential index, at each control volume by taking the logarithm of the power-law velocity profile (Eq. 2.1),

$$\begin{bmatrix} 1 & \log\left(x_{i-(N-2)}\right) \\ 1 & \log\left(x_{i-(N-1)}\right) \\ \vdots & \vdots \\ 1 & \log(x_i) \\ \vdots & \vdots \\ 1 & \log\left(x_{i+(N-1)}\right) \\ 1 & \log\left(x_{i+(N-2)}\right) \end{bmatrix} \begin{bmatrix} \log(k_i) \\ m_i \end{bmatrix} = \begin{bmatrix} \log\left(U_{e,i-(N-2)}\right) \\ \log\left(U_{e,i-(N-1)}\right) \\ \vdots \\ \log(U_{e,i}) \\ \vdots \\ \log\left(U_{e,i+(N-1)}\right) \\ \log\left(U_{e,i+(N-2)}\right) \end{bmatrix}. \tag{2.12}$$

The linear system in Eq. (2.12) can be written to be of arbitrary size, so long as the data from the control volume's neighbors are available. Due to the unstructured nature

of the code used, it is most computationally efficient to use three-point approximation, accessing only each control volume's nearest neighbors. Letting

$$A = \begin{bmatrix} 1 & \log\left(x_{i-(N-2)}\right) \\ 1 & \log\left(x_{i-(N-1)}\right) \\ \vdots & \vdots \\ 1 & \log(x_i) \\ \vdots & \vdots \\ 1 & \log\left(x_{i+(N-1)}\right) \\ 1 & \log\left(x_{i+(N-2)}\right) \end{bmatrix}, \tag{2.13}$$

$$\vec{x} = \begin{bmatrix} \log(k) \\ m \end{bmatrix}, \tag{2.14}$$

and

$$\vec{b} = \begin{bmatrix} \log\left(U_{e,i-(N-2)}\right) \\ \log\left(U_{e,i-(N-1)}\right) \\ \vdots \\ \log(U_{e,i}) \\ \vdots \\ \log\left(U_{e,i+(N-1)}\right) \\ \log\left(U_{e,i+(N-2)}\right) \end{bmatrix}, \tag{2.15}$$

then the normal equations,

$$A^T A\vec{x} = A^T\vec{b}, \tag{2.16}$$

can be solved to find the least-squares solution to the regression problem. Once m, and therefore β, is computed, first-order interpolation can be done to calculate $f''(0)$ using the values in Table 1, which are found by numerically integrating the Falkner-Skan equation. For the model problems studied in this report, coarse simulations will be done at resolutions such that the laminar boundary layer is subgrid in the entire computational domain. This allows for the estimation of k and m to be based simply on the information contained on the first control volume normal to the wall.

2.2. *Simulation details*

The calculations in this report are performed using the charLES solver. CharLES is a cell-centered, finite-volume code that solves the compressible Navier-Stokes equations on arbitrary unstructured meshes (Brès *et al.* 2018). It uses a third-order Runge-Kutta scheme for time advancement, and a nondissipative, energy- and entropy-conserving, second-order spatial discretization. All simulations performed for this report are two dimensional and nondimensionalized. The flow is assumed to be an ideal gas with $\gamma = 1.4$. Reference conditions for the speed of sound, temperature, density, and pressure are

$$c = 1, \quad T = 1, \quad \rho = 1, \quad p = \frac{1}{\gamma}. \tag{2.17}$$

We note that the solution in the vicinity of the outlet has been found to be affected

β	$f''(0)$
2.0000	1.687218
1.0000	1.232588
0.5000	0.927680
0.0000	0.469600
-0.1000	0.319270
-0.1200	0.281761
-0.1500	0.216362
-0.1800	0.128636
-0.1988	0.005216

TABLE 1. Corresponding values of β and $f''(0)$ for Falkner-Skan wedge flows. The local value of β is computed at each control volume associated with the boundary using a least-squares approximation. The values of this table are used in a first-order interpolation method to compute $f''(0)$ for intermediate values of β (Kuo 2005).

by the Navier-Stokes characteristic boundary condition (NSCBC) closure. In the second model problem studied, the inlet conditions lead to a small region of flow reversal near the symmetry plane, where it is inappropriate to apply the new wall model. We have therefore truncated the domains shown in the plots below.

3. Model problems

This section describes the performance of the Falkner-Skan-based wall model for two model problems, stagnation flow (also known as the Hiemenz problem) and a spatially varying pressure-gradient flow.

3.1. *Stagnation flow*

The proposed model was first applied to a stagnation flow configuration, corresponding to $\beta = m = 1$. This flow was chosen because it appears in many engineering problems and can be used as a model for the leading-edge region of an airfoil. Therefore, it is applicable to the goal of applying this wall model to reduce the computational cost of realistic airfoil simulations. Moreover, since the flow and the proposed Falkner-Skan wall model (FSWM) boundary condition are directly compatible, it serves as a good case to test the numerical implementation of the boundary condition. A schematic of the problem is shown in Figure 2. We have defined x_t to be the coordinate in the wall-tangential direction and x_n to be the wall-normal coordinate. The computational domain is half of a plane stagnation flow, enforced by a slip boundary condition on the $x_t = 0$ boundary. The inlet is placed at $x_n = 0$ and an NSCBC boundary condition (Poinsot & Lele 1992) is used at $x_t = L_t$.

The similarity solution for Hiemenz flow is solved numerically to generate the profiles of U_n and U_t. The profiles for T and ρ are corrected from being uniform everywhere in the domain with the isentropic flow relations to account for compressibility effects. The inlet profiles at $x_n = 0$ are shown in Figure 3. The only parameters necessary to fully define the Hiemenz problem are the viscosity ν and the strain rate k. The solution is normalized such that the boundary layer thickness is $\delta_{99} = 1$. The values of k and ν are

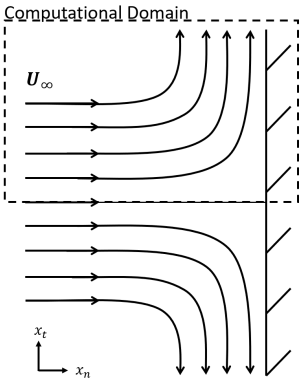

FIGURE 2. Schematic description of a flow against a vertical flat plate (Hiemenz flow). The computational domain is shown by the dashed box.

$$k = 2.3 \cdot 10^{-3}, \quad \nu = 3.978 \cdot 10^{-4}. \tag{3.1}$$

The Reynolds number is $Re_{\delta_{99}} = 840$ at the outlet. The size of the computational domain is $L_t = 150$ in the wall-tangential direction and $L_n = 20$ in the wall-normal direction. For the direct numerical simulation (DNS), the wall-tangential direction has uniform grid spacing with $N_t = 150$, and the wall-normal direction has hyperbolic tangent clustering with a ratio of $x_n/\Delta x_{wall} = 20$ and $N_n = 128$. Convergence is verified by comparing the DNS results with the semi-analytical solution of the Falkner-Skan equation. The FSWM was tested on a coarse grid with uniform spacing in both the streamwise and wall-normal directions, with $N_n = 5$ and $N_t = 150$. The comparison of boundary layer profiles between the DNS result and the FSWM calculation at several stations along the wall is shown in Figure 4. Excellent agreement throughout the entire domain can be seen, except at the station nearest to the outlet. In Figure 5, we show the stress calculated from using three different boundary conditions on the coarse simulation, no slip, FSWM, and the turbulent boundary layer equilibrium wall model (EQWM) (Bose & Park 2018). The comparison to the EQWM is important because in a typical large-scale WMLES containing laminar, transitional, and turbulent flow regimes, the EQWM would be applied to all wall boundaries. Figure 5 demonstrates the improved prediction of wall stress when the FSWM is used rather than using a no slip condition or the EQWM.

3.2. *Spatially varying pressure-gradient boundary layer*

To test the model in a more general setting, we applied the FSWM to flow over a flat plate with a spatially varying edge pressure gradient (Figure 6). The problem is intended to assess the validity of the local self-similarity assumption for a more general flow. An exponentially growing and decaying injection wall-normal velocity distribution is prescribed along the left boundary of the computational domain to create a favorable-to-adverse pressure gradient. The normal velocity distribution is given by

$$U_n(y) = -u_0 \bar{x} \exp\left(\frac{1}{2} - \frac{1}{2}\bar{x}^2\right), \tag{3.2}$$

with

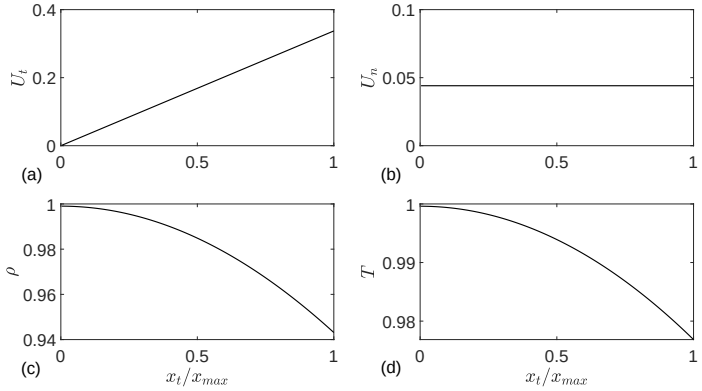

FIGURE 3. Inlet profiles used to initialize the stagnation flow case in charLES. The profiles are (a) wall-tangential velocity, (b) wall-normal velocity, (c) density, and (d) temperature.

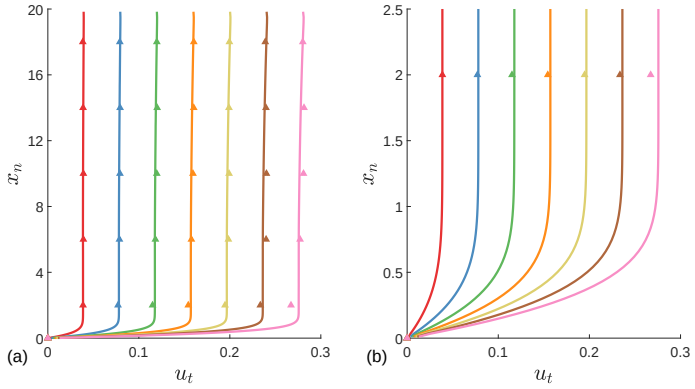

FIGURE 4. Comparison of boundary layer profiles between coarse FSWM (symbols) and DNS calculations (solid lines). From left to right, the stations correspond to $x_t = 17.50,\ 35.50,\ 53.50,\ 71.50,\ 89.50,\ 107.50$ and 125.50. (a) Entire domain. (b) Zoomed-in perspective.

$$\bar{x} = \frac{x - x_s}{\Delta x_s \exp(-1/2)}, \tag{3.3}$$

where x_s is the location where the wall-normal velocity returns to zero, Δx_s is the representative width of the injection region, and u_0 is the maximal amplitude of the velocity field.

A profile of $U_t(y)$ satisfying continuity is found analytically by finding the inviscid solution of a uniform flow subjected to the suction-injection profile U_n along $x_n = L_n$, with no penetration along the wall at $x_n = 0$ (see Karp & Hack 2020). The size of the computational domain is $L_t = 100$ along the wall-tangential direction and $L_n = 20$ in the wall-normal direction. For the DNS calculation, a uniform mesh distribution with $N_t = 200$ is used along the wall-tangential direction and a hyperbolic tangent clustering with a ratio of $\Delta x_n/\Delta x_{wall} = 20$ and $N_n = 256$ is used along the wall-normal direction. For the presented results, the maximum inlet Mach number is $Ma = 0.05$, $x_s = 50$, and $\Delta x_s = 30$. The Reynolds number based on $U_{e,max}$ and $\delta_{99,min}$ is $Re = 450$. The

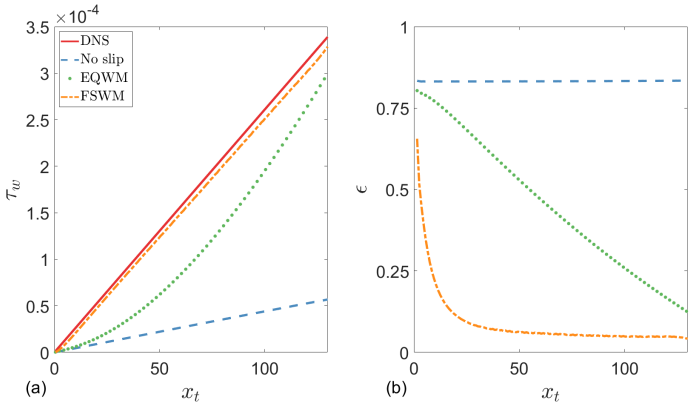

FIGURE 5. (a) Wall stress predicted by different boundary conditions for the coarse simulation: no slip (dashed line), EQWM (dotted line), and FSWM (dot-dashed line). The DNS (solid line) is given for reference. (b) The associated error.

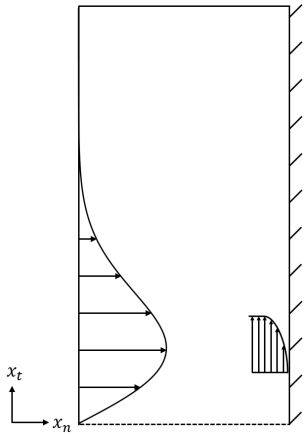

FIGURE 6. Schematic of a spatially varying pressure-gradient boundary layer flow.

inlet condition chosen, shown in Figure 7, provides a favorable pressure gradient near the symmetry plane of the domain, followed by a mildly adverse gradient toward the end of the domain. The boundary layer thickness from the DNS is shown in Figure 8, where we report a peak value of $\delta_{99} \approx 1.08$. The model is tested on a coarse, equally spaced grid that has a resolution of $N_t = 50$ and $N_n = 8$ in the wall-parallel and wall-normal directions, respectively. Therefore, the boundary layer is entirely subgrid in the coarse simulations.

Figure 9 compares the wall shear obtained from the DNS calculation with that from simulations run on the coarse mesh using no slip, EQWM, and FSWM boundary conditions. Similar to the results in the case of plane stagnation flow, the FSWM boundary condition offers a better prediction of the wall stress than the EQWM and no slip boundary conditions. Both the no slip and EQWM boundary conditions fail to capture the overall shape of the stress distribution, and instead the shear stress simply monotonically increases throughout the computational domain. By contrast, the FSWM performs

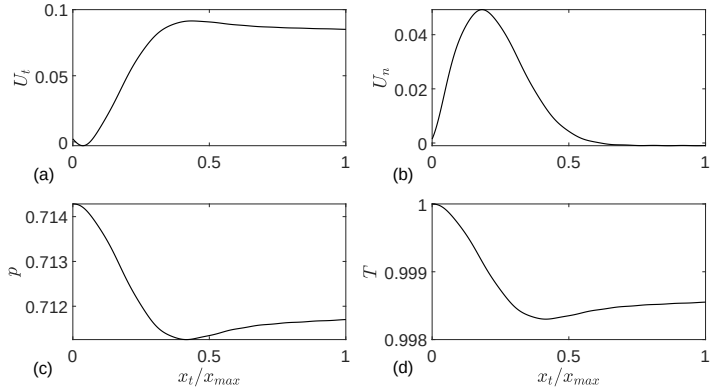

FIGURE 7. Inlet profiles used to initialize the spatially varying pressure-gradient boundary layer flow case in charLES. (a) wall-tangential velocity, (b) wall-normal velocity, (c) pressure, and (d) temperature.

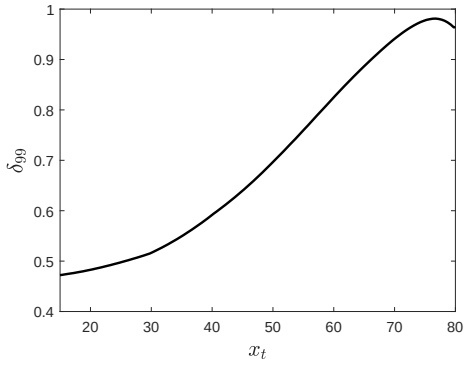

FIGURE 8. The δ_{99} boundary layer thickness from the DNS.

well in capturing the initial increase in wall stress, peaking near the center of the domain and then decreasing toward the outlet.

Figure 10 plots the estimated values of k and m for the DNS and FSWM simulations at the boundary layer edge. We observe reasonable agreement between the two curves, particularly toward the center of the domain. Potential improvements could be made by using a more robust outlet boundary condition, increasing the stencil width of the least-squares approximation, or developing an alternative, more robust method for estimating the power-law parameters.

4. Conclusions

An algebraic wall model for laminar flows based on the similarity solution to Falkner-Skan flows is developed. The model produced accurate results on the under-resolved grids of the two test cases. In the case of stagnation flow, the FSWM nearly perfectly recovered the DNS wall stress. For the pressure-gradient boundary layer, the FSWM strongly tracked the DNS wall stress, whereas the EQWM missed the trend of the curve entirely. We also saw good agreement in the Falkner-Skan power-law parameters between the

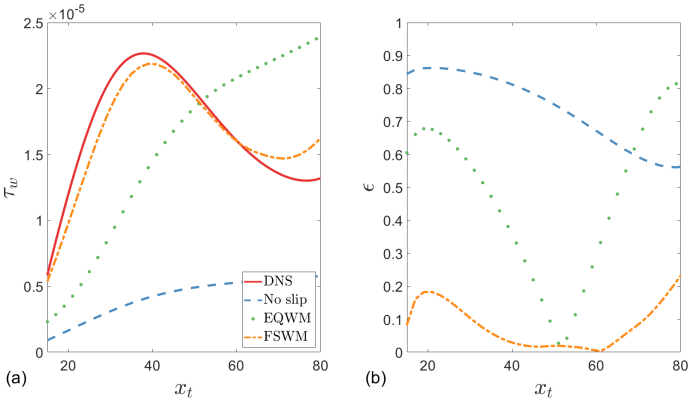

FIGURE 9. (a) Wall stress predicted by different boundary conditions for the coarse simulation: no slip (dashed line), EQWM (dotted line), and FSWM (dot-dashed line). The DNS (solid line) is given for reference. (b) The associated error.

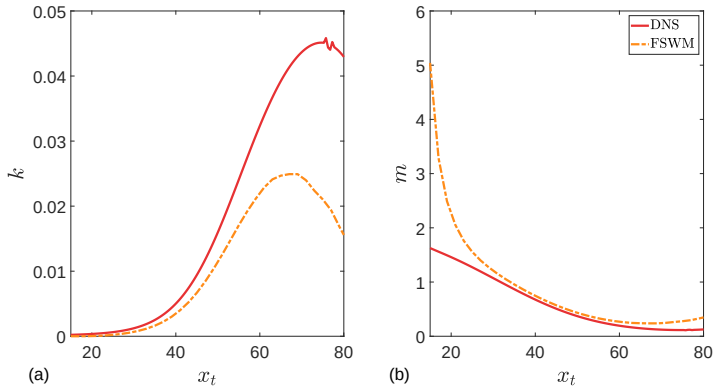

FIGURE 10. A comparison of the DNS (solid line) and the FSWM simulation (dashed line) of the Falkner-Skan variables (a) k and (b) m.

DNS and coarse grid simulations, indicating that the assumption of local self-similarity for arbitrary laminar boundary layers is valid and that knowledge of the boundary layer edge velocity U_e is sufficient information to form the boundary condition. This constitutes the initial stage in the development of a wall model for large-eddy simulations of flows that simultaneously contain regions of laminar, transitional, and turbulent flows. The formulation herein is based on the assumption of local self-similarity of laminar boundary layers such that at each streamwise location, the flow can be thought of as a Falkner-Skan wedge flow. A least-squares solve is used to approximate the Falkner-Skan power-law parameters k and m using local cell data. The natural extension of this work will be to apply the newly developed boundary condition to flow over a natural laminar flow airfoil. The findings in this report suggest that this wall model serves as a way to efficiently improve the predicted wall shear stress and boundary layer profiles in under-resolved, laminar regions of flow.

Acknowledgments

This investigation was funded by the Stanford Engineering Graduate Fellowship and by NASA (grant #NNX15AU93A). The authors acknowledge use of computational resources from the Certainty cluster awarded by the National Science Foundation to CTR. The authors are grateful to Sanjeeb Bose for useful suggestions.

REFERENCES

Bose, S. T. & Park, G. I. 2018 Wall-modeled large-eddy simulation for complex turbulent flows. *Annu. Rev. Fluid Mech.* **50**, 535–561.

Brès, G. A., Bose, S. T., Emory, M., Ham, F. E., Schmidt, O. T., Rigas, G. & Colonius, T. 2018 Large-eddy simulations of co-annular turbulent jet using a Voronoi-based mesh generation framework. *AIAA Paper* 2018-3302.

Drela, M. & Giles, M. B. 1987 Viscous-inviscid analysis of transonic and low Reynolds number airfoils. *AIAA J.* **25**, 1347–1355.

Goc, K., Bose, S. & Moin, P. 2020 Wall-modeled large eddy simulation of an aircraft in landing configuration. *AIAA Paper* 2020-3002.

Karp, M. & Hack, M. J. P. 2020 Optimal suppression of a separation bubble in a laminar boundary layer. *J. Fluid Mech.* **892**, A23.

Kuo, B.-L. 2005 Heat transfer analysis for the Falkner-Skan wedge flow by the differential transformation method. *Int. J. Heat Mass Tran.* **48**, 5036–5046.

Ladson, C. L., Hill, A. S., & Johnson, W. 1987 Pressure distributions from high Reynolds number transonic tests of an NACA 0012 airfoil in the Langley 0.3-meter transonic cryogenic tunnel. NASA Tech. Memorandum 100526.

Marques, A. N. & Wang, Q. 2017 Integral formulation of under-resolved near-wall scales for coarse-grid LES. *AIAA Paper* 2017-0980.

Poinsot, T. J. & Lele, S. K. 1992 Boundary conditions for direct simulations of compressible viscous flows. *J. Comput. Phys.* **101**, 104–129.

Slotnick, J., Khodadoust, A., Alonso, J. & Darmofal, D. 2014 CFD Vision 2030 Study: A Path to Revolutionary Computational Aerosciences. NASA/CR-2014-218178.

White, F. M. & Corfield, I. 2006 *Viscous Fluid Flow*, McGraw-Hill.